Monatsh Chem 139, 481–487 (2008)
DOI 10.1007/s00706-007-0796-x
Printed in The Netherlands

Monatshefte für Chemie
Chemical Monthly

Rare earth metal-rich indides RE_4IrIn (RE = Gd–Er), RE_4IrInO$_{0.25}$ (RE = Gd, Er), and RE_4TIn$_{1-x}$Mg$_x$ (RE = Y, Gd; T = Rh, Ir)

Roman Zaremba, Ute Ch. Rodewald, Rolf-Dieter Hoffmann, Rainer Pöttgen

Institut für Anorganische und Analytische Chemie, Westfälische Wilhelms-Universität Münster, Münster, Germany

Received 26 June 2007; Accepted 3 September 2007; Published online 21 March 2008

Abstract The rare earth-transition metal-indides RE_4IrIn (RE = Gd–Er) and the solid solutions RE_4TIn$_{1-x}$Mg$_x$ (RE = Y, Gd; T = Rh, Ir) were prepared by arc-melting of the elements and subsequent annealing. The rare earth sesquioxides were used as oxygen source for the suboxides RE_4IrInO$_{0.25}$ (RE = Gd, Er). Single crystals of the indides were grown *via* slowly cooling of the samples and they were investigated *via* X-ray powder diffraction and single crystal diffractometer data: Gd$_4$RhIn type, $F\bar{4}3m$, a = 1372.3(6) pm for Gd$_4$IrIn, a = 1365.3(6) pm for Tb$_4$IrIn, a = 1356.7(4) pm for Dy$_4$IrIn, a = 1353.9(4) pm for Ho$_4$IrIn, a = 1344.1(4) pm for Er$_4$IrIn, a = 1370.3(5) pm for Y$_4$RhIn$_{0.54}$Mg$_{0.46}$, a = 1375.6(5) pm for Gd$_4$IrIn$_{0.55}$Mg$_{0.45}$, a = 1373.0(3) pm for Gd$_4$IrInO$_{0.25}$, and a = 1345.1(4) pm for Er$_4$IrInO$_{0.25}$. The rhodium and iridium atoms have a trigonal prismatic rare earth coordination. Condensation of the RhRE_6 and IrRE_6 prisms leads to three-dimensional networks which leave voids that are filled by regular In$_4$ or mixed In$_{4-x}$Mg$_x$ tetrahedra. The indium (magnesium) atoms have twelve nearest neighbors (3In(Mg) + 9RE) in icosahedral coordination. The rare earth atoms build up a three-dimensional, adamantane-like network of condensed, edge and face-sharing octahedra. For Gd$_4$IrInO$_{0.25}$ and Er$_4$IrInO$_{0.25}$ the $RE1_6$ octahedra are filled with oxygen. The crystal chemical peculiarities of these rare earth rich compounds are discussed.

Keywords Rare earth compounds; Indides; Suboxides; Crystal chemistry.

Introduction

During our systematic phase analytical studies of rare earth metal-rich indides RE_xT_yIn$_z$ (RE = rare earth metal; T = late transition metal) [1–3, and references therein], we discovered the new structure type Gd$_4$RhIn (space group $F\bar{4}3m$, Z = 16) [4] within the series of RE_4RhIn indides. Besides these indides, the Gd$_4$RhIn structure type also exists for the magnesium based series RE_4CoMg [5], RE_4RhMg [6], RE_4RuMg [7], and the cadmium compounds RE_4TCd (RE = Tb, Dy, Ho and T = Co, Rh) [8].

The striking structural motifs in this new structure type are transition metal centered trigonal prisms of the rare earth atoms. The latter are condensed *via* common edges and corners, forming a three-dimensional network with cubic symmetry, $\bar{4}3m$. The voids between these trigonal prisms are filled by X_4 tetrahedra (X = Mg, In, Cd) in *fcc* packing and by the $RE1$ atoms. The latter connect the RE_6T networks and the X_4 units. The X-X distances within the X_4 tetrahedra are mostly smaller than in elemental magnesium, cadmium, or indium [9]. The crystal

Correspondence: Rainer Pöttgen, Institut für Anorganische und Analytische Chemie, Westfälische Wilhelms-Universität Münster, Germany. E-mail: pottgen@uni-muenster.de

chemical details of this new structure type and details on chemical bonding are discussed in Refs. [4] and [5].

The magnesium based compounds show some peculiarities. The *RE*1 positions that do not participate in the three-dimensional network of condensed trigonal prisms show solid solutions with magnesium leading to compositions $RE_{4-x}T\mathrm{Mg}_{1+x}$ [5, 6]. Furthermore, some of the magnesium compounds show small defects on the transition metal site. These structural modifications strongly influence the magnetic properties. Since this structure type exhibits empty octahedral voids formed by the rare earth elements, the hydrogenation behavior has been tested exemplarily for Gd_4NiMg. At room temperature and a hydrogen pressure of 4 MPa Gd_4NiMg absorbs up to eleven hydrogen atoms per formula unit [10].

We have now extended our investigations of the Gd_4RhIn type materials. Herein we report on the synthesis and structures of the series of iridium containing intermetallics RE_4IrIn (RE = Gd–Er) as well as the structures of $Y_4RhIn_{0.54}Mg_{0.46}$ and $Gd_4IrIn_{0.55}Mg_{0.45}$, where we tested for In/Mg substitution within the X_4 tetrahedra. The experimental data gave a hint for oxygen contamination for some of the RE_4IrIn compounds. This was experimentally proved through the synthesis of the new suboxides $Gd_4IrInO_{0.25}$ and $Er_4IrInO_{0.25}$.

Results and discussion

The series of RE_4IrIn indides has been synthesized and structurally characterized on the basis of powder and single crystal X-ray data. These indides are isotypic with Gd_4RhIn [4], space group $F\bar{4}3m$. The cell volumes decrease from the gadolinium to the erbium compound as expected from the lanthanoid contraction. The striking structural features are the iridium-centered trigonal prisms formed by the *RE*2 and *RE*3 atoms. The latter are condensed *via* common edges and corners, leading to a rigid, covalently bonded network with adamantane-like symmetry. The *RE*1 atoms are capping the trigonal prisms on the rectangular face, leading to coordination number 9 for the iridium atoms, a coordination typically observed in rare earth-transition metal-indides [16]. The indium atoms build up In_4 tetrahedra which fill voids left by the network of condensed trigonal prisms.

Chemical bonding in Gd_4RhIn type compounds has exemplarily been investigated for La_4CoMg [5] and La_4RuMg [6]. These calculations clearly revealed that the *RE*–*T* interactions are the strongest ones in these structures. The crystal chemistry of these compounds has been discussed in detail in all previous work [4–6]. Herein we focus on the oxygen contanimation in the series of RE_4IrIn compounds and the formation of solid solutions.

As already discussed for the series of RE_4RhIn indides [4], the rare earth atoms build up a network of empty RE_6 octahedra. Several RE_4RhIn and RE_4IrIn crystals investigated revealed higher residual peaks at those positions. This leaves the possibility, that some of these voids in such crystals might be partially filled with light element atoms, *e.g.* nitrogen or oxygen. In our case the Gd_6 octahedra at the special position 4*c* are filled.

In a first synthesis step, oxygen was introduced in two samples through the sesquioxides RE_2O_3, and chemical analysis of the bulk samples (see above) clearly revealed the oxygen content (X-ray powder data revealed slightly larger lattice parameters for the oxygen containing samples). Nitrogen was only observed as a trace. Single crystals of those samples showed full oxygen occupancy of the octahedral voids formed by the *RE*1 atoms. In all previous experiments, the oxygen contamination might have resulted from oxidic impurities on the surface of the used rare earth lumps. In this regard it is interesting to note, that crystals grown from samples of the starting composition *RE*:*T*:In of 4.1:1:1 did not reveal higher residual peaks. This might be a hint that the excess rare earth element might have trapped the light element impurities. So far, this behavior was not observed for the magnesium and cadmium based compounds [5–8]. Especially in the case of magnesium, the high lattice energy of MgO prevents incorporation of oxygen into the $RE_4T\mathrm{Mg}$ compounds. Keeping the experimentally proved small oxygen content in mind, it is impossible to differentiate whether the data sets of the RE_4IrIn compounds reveal some systematical errors or a trace amount of oxygen within the *RE*1 octahedra. We will now start more detailed investigations on the solid solution $Gd_4IrIn \rightarrow Gd_4IrInO_{0.25}$ with respect to physical properties. The differing oxygen content will certainly influence the electron density at the gadolinium atoms and thus the magnetic behavior.

In a second experiment we have tested the indium-magnesium substitution within the tetrahedral subunits. The structures of $Y_4RhIn_{0.54}Mg_{0.46}$ and $Gd_4IrIn_{0.55}Mg_{0.45}$ have been refined on the basis of single crystal data. Also these data sets revealed no enhanced residual peaks, most likely due to the MgO trap. Furthermore, the indium-magnesium substitution is a suitable tool to influence the magnetic properties, since we can reduce the valence electron concentration with increasing magnesium content. Recent experiments on the solid solution $CeAuIn_{1-x}Mg_x$ and related compounds [17, 18, and references therein] have clearly shown the influence of the valence electron concentration on the magnetic properties.

Finally we describe the oxygen coordination within the suboxide $Gd_4IrInO_{0.25}$ (Fig. 1). The oxygen centered $OGd1_6$ octahedra (259 pm Gd1-O) are surrounded by twelve $IrGd_6$ trigonal prisms in a motif resembling the close-packed structures (cuboctahedron). Such oxygen-filled rare earth octahedra have been observed also in the $RE_{12}Fe_{32}O_2$ phases [19, 20], similar to $Ca_6Ag_{16}N$ [21].

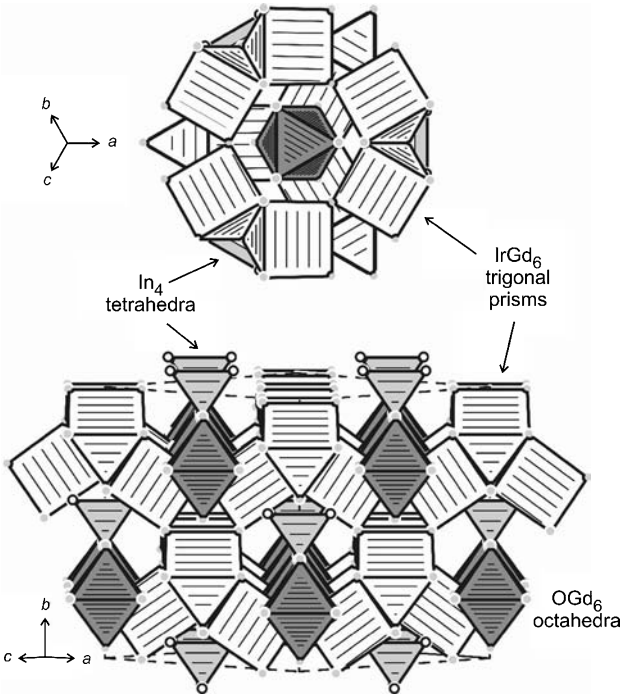

Fig. 1 The crystal structure of $Gd_4IrInO_{0.25}$. Gadolinium and indium atoms are drawn as medium gray and open circles, respectively. The iridium and oxygen atoms are hidden within the trigonal prisms and the octahedra. The top drawing shows the coordination of the iridium filled trigonal prisms around the oxygen centered octahedra (view along the threefold axis). At the bottom a view of the structure approximately along the [101] direction is given, emphasizing the condensed Gd_6Ir prisms, the OGd_6 octahedra and the In_4 tetrahedra

Experimental

Synthesis

Starting materials for the preparation of the RE_4IrIn, $RE_4TIn_{1-x}Mg_x$ and $RE_4IrInO_{0.25}$ samples were ingots of the rare earth metals (Johnson Matthey, Chempur or Kelpin), rhodium and iridium powder (*ca.* 200 mesh, Degussa-Hüls), indium tear drops (Johnson Matthey), a magnesium rod (Johnson Matthey, 16 mm), Gd_2O_3 (Chempur), and Er_2O_3 (Chempur), all with stated purities better than 99.9%. The surface of the magnesium rod was cut on a turning lathe in order to remove surface impurities. The rare earth metal ingots were cut into smaller pieces and arc-melted [11] to small buttons (*ca.* 400 mg) under an argon atmosphere. The argon was purified over titanium sponge (900 K), silica gel, and molecular sieves. The premelting procedure reduces shattering during the subsequent reactions with iridium and indium. The rare earth metal buttons were then mixed with cold-pressed pellets (Ø 6 mm) of iridium and pieces of the indium tear drops in the ideal 4:1:1 atomic ratio. The mixtures were reacted in the arc-furnace and remelted three times to ensure homogeneity. For synthesis of the oxides, an appropriate amount of the rare earth sesquioxide was used and these samples were also synthesized *via* arc-melting. The weight losses after the melting procedures were smaller than 0.5%.

The magnesium based samples could not be synthesized *via* arc-melting, since the low boiling temperature of magnesium would result in a large mass loss. For the synthesis of the $RE_4TIn_{0.5}Mg_{0.5}$ (T = Rh, Ir) samples with yttrium and gadolinium, the elements were weighed in the ideal atomic ratio and sealed in tantalum tubes. The ampoules were then heated in a water-cooled sample chamber of an induction furnace with the same annealing sequence as for the ternary magnesium based RE_4TMg compounds [5–7]. All polycrystalline samples are brittle and stable in air over months. Finely ground powders are dark gray and single crystals exhibit metallic luster.

For single crystal growth the indides were treated *via* a special annealing sequence in tantalum crucibles as reported earlier for the RE_4RhIn series [4]. After cooling, the samples could easily be separated from the tantalum containers. No reaction of the samples with tantalum could be detected.

Scanning electron microscopy

The single crystals investigated on the diffractometers and the bulk samples have been analyzed by EDX measurements using a LEICA 420 I scanning electron microscope with the rare earth trifluorides, iridium, MgO, and InAs as standards. Since the crystals were mounted by beeswax on glass fibres,

they were first coated with a thin carbon film. The bulk samples were previously embedded in a metacrylate matrix and the surface was polished with different silica and diamond pastes. The surface remained unetched for the EDX measurements. No impurity elements were detected and the analyses were in agreement with the ideal 4:1:1 composition. For the magnesium containing samples the Mg:In ratio was close to the one refined from the X-ray data. The oxygen content of the $Gd_4IrInO_{0.25}$ and $Er_4IrIn_{0.25}$ samples could not be determined reliably (resolution of the instrument).

Table 1 Lattice parameters (*Guinier* powder data) of the ternary indium compounds RE_4IrIn and related compounds

Compound	a/pm	V/nm^3
Gd_4IrIn	1372.3(6)	2.5843
Tb_4IrIn	1365.3(6)	2.5450
Dy_4IrIn	1356.7(4)	2.4972
Ho_4IrIn	1353.9(4)	2.4819
Er_4IrIn	1344.1(4)	2.4283
$Gd_4IrInO_{0.25}$	1373.0(3)	2.5883
$Er_4IrInO_{0.25}$	1345.1(4)	2.4337
$Y_4RhIn_{0.54}Mg_{0.46}$	1370.3(5)	2.5730
$Gd_4IrIn_{0.55}Mg_{0.45}$	1375.6(5)	2.6030

X-Ray film data and structure refinements

The RE_4IrIn, $RE_4TIn_{1-x}Mg_x$ and RE_4IrInO_x samples were characterized *via Guinier* powder patterns using Cu Kα_1 radiation and α-quartz ($a = 491.30$, $c = 540.46$ pm) as an internal standard. The *Guinier* camera was equipped with an imaging plate system (Fujifilm BAS-1800). The cubic lattice parameters (Table 1) were deduced from least-squares fits of the powder data. The correct indexing of the experimental patterns was ensured through intensity calculations [12], taking the atomic positions obtained from the structure refinements. Based on the powder patterns, the samples were obtained in X-ray pure form.

Irregularly shaped single crystals of Gd_4IrIn, Tb_4IrIn, Ho_4IrIn, Er_4IrIn, $Y_4RhIn_{0.54}Mg_{0.46}$, $Gd_4IrIn_{0.55}Mg_{0.45}$, $Gd_4IrInO_{0.25}$, and $Er_4IrInO_{0.25}$ were selected from the annealed samples and examined by *Laue* photographs on a *Buerger* precession camera (equipped with an imaging plate system Fujifilm BAS-1800) in order to establish suitability for intensity data collection. Intensity data were collected in oscillation mode on a *Stoe* IPDS-II image plate diffractometer using monochromatized MoK_α radiation (71.073 pm). Numerical absorption corrections were applied to the data sets. All relevant crystallographic details for the data collections and evaluations are listed in Tables 2 and 3.

All data sets revealed only the systematic extinctions of a face-centered cubic lattice. In agreement with the earlier

Table 2 Crystal data and structure refinement for RE_4IrIn, Gd_4RhIn type, space group $F\bar{4}3m$, $Z = 16$

Empirical formula	Gd_4IrIn	Tb_4IrIn	Ho_4IrIn	Er_4IrIn
Molar mass	936.02 g/mol	942.70 g/mol	966.74 g/mol	976.06 g/mol
Unit cell dimensions	Table 1	Table 1	Table 1	Table 1
Calculated density	9.62 g/cm^3	9.84 g/cm^3	10.35 g/cm^3	10.68 g/cm^3
Crystal size	$10 \times 15 \times 90$ µm^3	$10 \times 90 \times 100$ µm^3	$20 \times 60 \times 70$ µm^3	$20 \times 40 \times 90$ µm^3
Detector distance	60 mm	60 mm	60 mm	60 mm
Exposure time	5 min	5 min	5 min	5 min
ω range; increment	0–180°; 1.0°	0–180°; 1.0°	0–180°; 1.0°	0–180°; 1.0°
Integr. param. A, B, EMS	13.5; 3.5; 0.012	13.5; 3.5; 0.012	14.0; 4.0; 0.036	14.5; 2.9; 0.043
Transm. ratio (max/min)	3.11	9.02	7.72	3.14
Absorption coefficient	64.3 mm^{-1}	68.1 mm^{-1}	75.3 mm^{-1}	80.1 mm^{-1}
F(000)	6112	6176	6304	6368
θ range	2°–30°	2°–30°	3°–30°	2°–30°
Range in *hkl*	±19, ±17, +19	±19, ±19, ±18	±18, ±18, ±18	±18, ±18, ±18
Total no. reflections	3551	3230	4889	2064
Independent reflections	404 ($R_{int} = 0.082$)	392 ($R_{int} = 0.040$)	407 ($R_{int} = 0.081$)	355 ($R_{int} = 0.084$)
Reflections with $I > 2\sigma(I)$	315 ($R_\sigma = 0.078$)	364 ($R_\sigma = 0.030$)	370 ($R_\sigma = 0.043$)	274 ($R_\sigma = 0.088$)
Data/parameters	404/19	392/19	407/19	355/20
Goodness-of-fit on F^2	0.747	0.951	0.919	0.802
Final R indices [$I > 2\sigma(I)$]	$R1 = 0.023$	$R1 = 0.018$	$R1 = 0.023$	$R1 = 0.031$
	$wR2 = 0.044$	$wR2 = 0.037$	$wR2 = 0.044$	$wR2 = 0.056$
R indices (all data)	$R1 = 0.035$	$R1 = 0.021$	$R1 = 0.028$	$R1 = 0.046$
	$wR2 = 0.045$	$wR2 = 0.037$	$wR2 = 0.045$	$wR2 = 0.058$
Extinction coefficient	0.000088(6)	0.000107(6)	0.000337(14)	0.000124(8)
Flack parameter	−0.04(3)	−0.02(2)	−0.01(3)	–
BASF	–	–	–	0.11(5)
Largest diff. peak and hole	4.54/−1.84 e/Å^3	3.85/−1.29 e/Å^3	2.95/−2.31 e/Å^3	3.69/−2.32 e/Å^3

Table 3 Crystal data and structure refinement for $Gd_4IrInO_{0.25}$, $Er_4IrInO_{0.25}$, $Y_4RhIn_{0.54}Mg_{0.46}$, and $Gd_4IrIn_{0.55}Mg_{0.45}$; Gd_4RhIn type, space group $F\bar{4}3m$, $Z = 16$

Empirical formula	$Gd_4IrInO_{0.25}$	$Er_4IrInO_{0.25}$	$Y_4RhIn_{0.54}Mg_{0.46}$	$Gd_4IrIn_{0.55}Mg_{0.45}$
Molar mass	940.02 g/mol	980.06 g/mol	531.74 g/mol	895.57 g/mol
Unit cell dimensions	Table 1	Table 1	Table 1	Table 1
Calculated density	9.65 g/cm^3	10.70 g/cm^3	5.49 g/cm^3	9.14 g/cm^3
Crystal size	$20 \times 40 \times 110$ μm^3	$40 \times 80 \times 150$ μm^3	$15 \times 40 \times 90$ μm^3	$10 \times 30 \times 80$ μm^3
Detector distance	60 mm	60 mm	60 mm	60 mm
Exposure time	5 min	5 min	6 min	5 min
ω range; increment	0–180°; 1.0°	0–180°; 1.0°	0–180°; 1.0°	0–180°; 1.0°
Integr. param. A, B, EMS	13.0; 3.5; 0.012	13.5; 3.5; 0.012	13.5; 3.5; 0.014	13.5; 3.5; 0.012
Transm. ratio (max/min)	4.65	7.56	2.50	2.81
Absorption coefficient	64.3 mm^{-1}	79.9 mm^{-1}	40.0 mm^{-1}	62.4 mm^{-1}
$F(000)$	6144	6400	3728	5847
θ range	2°–35°	2°–35°	2°–34°	2°–30°
Range in hkl	±22, ±20, +22	±21, ±21, ±21	±21, ±21, ±21	±19, ±19, ±19
Total no. reflections	9808	9232	8899	6884
Independent reflections	615 ($R_{int} = 0.066$)	589 ($R_{int} = 0.069$)	554 ($R_{int} = 0.114$)	429 ($R_{int} = 0.083$)
Reflections with $I > 2\sigma(I)$	552 ($R_\sigma = 0.039$)	548 ($R_\sigma = 0.031$)	422 ($R_\sigma = 0.077$)	354 ($R_\sigma = 0.059$)
Data/parameters	615/20	589/21	554/21	429/20
Goodness-of-fit on F^2	0.964	1.088	0.745	0.782
Final R indices [$I > 2\sigma(I)$]	$R1 = 0.027$	$R1 = 0.028$	$R1 = 0.030$	$R1 = 0.023$
	$wR2 = 0.054$	$wR2 = 0.060$	$wR2 = 0.041$	$wR2 = 0.036$
R indices (all data)	$R1 = 0.032$	$R1 = 0.031$	$R1 = 0.048$	$R1 = 0.034$
	$wR2 = 0.055$	$wR2 = 0.061$	$wR2 = 0.044$	$wR2 = 0.038$
Extinction coefficient	0.000197(10)	0.000304(16)	0.000160(11)	0.000045(4)
Flack parameter	−0.02(2)	–	–	−0.01(3)
BASF	–	0.49(3)	0.17(2)	–
Largest diff. peak and hole	2.59/−3.18 e/Å^3	4.97/−2.85 e/Å^3	1.32/−1.21 e/Å^3	2.67/−1.30 e/Å^3

investigations on the RE_4RhIn indides [4], space group $F\bar{4}3m$ was found to be the correct one. The atomic parameters of Gd_4RhIn [4] were used as starting values and the structures were refined using SHELXL-97 (full-matrix least-squares on F_o^2) [13] with anisotropic atomic displacement parameters for all sites. For the RE_4IrIn compounds, refinement of the occupancy parameters in separate series of least-squares cycles revealed no deviation from the ideal composition. For the crystals of the solid solutions $RE_4T\text{In}_{1-x}\text{Mg}_x$, the In/Mg ratio was refined as a least-squares variable in the final cycles, leading to the compositions $Y_4RhIn_{0.54}Mg_{0.46}$, $Gd_4IrIn_{0.55}Mg_{0.45}$ for the investigated crystals. Refinement of the correct absolute structures was ensured through refinement of the *Flack* parameters [14, 15]. Several crystals revealed partial merohedral twinning *via* the matrix 1/3 −2/3 2/3, 2/3 −1/3 −2/3, 2/3 2/3 1/3, and this was accounted for during data integration.

Two crystals of the initial compositions Gd_4IrIn and Er_4IrIn revealed high residual peaks at the special positions 1/4 1/4 1/4 and 3/4 3/4 3/4. This position is an octahedral void built up by six Gd1 atoms. Such highly symmetrical sites can accumulate artifacts within a structure refinement leading to residual peaks. In the present case, refinement of these structures with an oxygen atom within the octahedral voids was possible and the resulting interatomic distances were reasonable. Subsequently we could also synthesize the oxygen containing samples. Analyses of the bulk samples *via* the hot gas extraction method (Mikroanalytisches Labor Pascher, Remagen) revealed oxygen contents (weight-%) of 0.17 (Gd sample) and 0.20 (Er sample), somewhat smaller than the calculated values of 0.85 and 0.81 for $Gd_4IrInO_{0.25}$ and $Er_4IrInO_{0.25}$, respectively. The formula does not imply a partial occupancy of oxygen (see Table 4); it is merely used for easier comparison. Only traces of nitrogen were detected. The crystal chemical consequences are discussed below. The slightly higher electron density on the 4*d* site of $Er_4IrInO_{0.25}$ most likely indicates that also systematic errors accumulate here.

Final difference *Fourier* syntheses revealed no significant residual peaks (Tables 2 and 3). The positional parameters and interatomic distances (exemplarily for $Gd_4IrInO_{0.25}$) are listed in Tables 4 and 5. Further details on the structure refinements may be obtained from Fachinformationszentrum Karlsruhe, D-76344 Eggenstein-Leopoldshafen (Germany), by quoting the Registry Nos. CSD-418266 (Gd_4IrIn), CSD-418269 (Tb_4IrIn), CSD-418270 (Ho_4IrIn), CSD-418265 (Er_4IrIn), CSD-418268 ($Y_4RhIn_{0.54}Mg_{0.46}$), CSD-418272 ($Gd_4IrIn_{0.55}Mg_{0.45}$) CSD-418271 ($Gd_4IrInO_{0.25}$) CSD-418267 ($Er_4IrInO_{0.25}$).

Table 4 Atomic coordinates and isotropic displacement parameters (pm^2) of RE_4IrIn. U_{eq} is defined as one third of the trace of the orthogonalized U_{ij} tensor. The displacement parameter of the oxygen position of $Er_4IrInO_{0.25}$ was fixed. Refinement of the occupancy parameter along with the displacement parameter was not possible

Atom	*Wyckoff* site	Occupancy/%	*x*	*y*	*z*	U_{eq}
Gd_4IrIn						
Gd1	24*g*	100	0.43910(9)	3/4	3/4	73(3)
Gd2	24*f*	100	0.80848(10)	0	0	55(3)
Gd3	16*e*	100	0.65107(7)	*x*	*x*	46(3)
Ir	16*e*	100	0.85857(6)	*x*	*x*	49(3)
In	16*e*	100	0.41791(11)	*x*	*x*	59(5)
Tb_4IrIn						
Tb1	24*g*	100	0.56032(6)	1/4	1/4	72(2)
Tb2	24*f*	100	0.19136(5)	0	0	49(2)
Tb3	16*e*	100	0.34922(4)	*x*	*x*	45(2)
Ir	16*e*	100	0.14147(3)	*x*	*x*	48(2)
In	16*e*	100	0.58217(6)	*x*	*x*	55(3)
Ho_4IrIn						
Ho1	24*g*	100	0.55994(7)	1/4	1/4	75(2)
Ho2	24*f*	100	0.19120(7)	0	0	52(2)
Ho3	16*e*	100	0.34913(5)	*x*	*x*	50(3)
Ir	16*e*	100	0.14144(5)	*x*	*x*	55(2)
In	16*e*	100	0.58277(9)	*x*	*x*	59(3)
Er_4IrIn						
Er1	24*g*	100	0.56059(12)	1/4	1/4	69(3)
Er2	24*f*	100	0.19143(11)	0	0	42(3)
Er3	16*e*	100	0.34953(9)	*x*	*x*	45(4)
Ir	16*e*	100	0.14162(8)	*x*	*x*	45(3)
In	16*e*	100	0.58304(14)	*x*	*x*	49(6)
$Gd_4IrInO_{0.25}$						
Gd1	24*g*	100	0.43888(6)	3/4	3/4	92(2)
Gd2	24*f*	100	0.80849(7)	0	0	67(2)
Gd3	16*e*	100	0.65090(4)	*x*	*x*	64(2)
Ir	16*e*	100	0.85848(4)	*x*	*x*	65(2)
In	16*e*	100	0.41807(7)	*x*	*x*	71(3)
O	4*c*	101(15)	1/4	1/4	1/4	130(66)
$Er_4IrInO_{0.25}$						
Er1	24*g*	100	0.56039(6)	1/4	1/4	99(2)
Er2	24*f*	100	0.19201(6)	0	0	69(2)
Er3	16*e*	100	0.34989(4)	*x*	*x*	66(2)
Ir	16*e*	100	0.14143(4)	*x*	*x*	68(2)
In	16*e*	100	0.58307(7)	*x*	*x*	73(3)
O	4*d*	143(10)	3/4	3/4	3/4	100
$Y_4RhIn_{0.54}Mg_{0.46}$						
Y1	24*g*	100	0.43667(8)	3/4	3/4	75(3)
Y2	24*f*	100	0.81120(9)	0	0	58(3)
Y3	16*e*	100	0.65270(7)	*x*	*x*	65(3)
Rh	16*e*	100	0.85804(6)	*x*	*x*	94(3)
In/Mg	16*e*	54.0(8)/46.0(8)	0.41797(9)	*x*	*x*	77(5)
$Gd_4IrIn_{0.55(1)}Mg_{0.45(1)}$						
Gd1	24*g*	100	0.56174(8)	1/4	1/4	83(2)
Gd2	24*f*	100	0.19046(8)	0	0	53(2)
Gd3	16*e*	100	0.34780(6)	*x*	*x*	45(3)
Ir	16*e*	100	0.14128(5)	*x*	*x*	58(2)
In/Mg	16*e*	55(1)/45(1)	0.58161(14)	*x*	*x*	71(10)

Table 5 Interatomic distances (pm), calculated with the powder lattice parameters of $Gd_4IrInO_{0.25}$. Standard deviations are given in parentheses. All distances within the first coordination spheres are listed

Gd1:	1	O	259.3(1)	Gd3:	3	Ir	285.6(1)
	2	In	327.6(1)		3	In	346.6(1)
	2	Gd3	349.0(1)		3	Gd1	349.0(1)
	2	Ir	349.0(1)		3	Gd2	364.2(1)
	4	Gd2	362.4(1)		3	Gd3	384.9(1)
	4	Gd1	366.7(2)	Ir:	3	Gd2	283.2(1)
Gd2:	2	Ir	283.2(1)		3	Gd3	285.6(1)
	2	In	349.4(1)		3	Gd1	349.0(1)
	4	Gd1	362.4(1)	In:	3	In	318.2(1)
	2	Gd3	364.2(1)		3	Gd1	327.6(1)
	4	Gd2	371.9(2)		3	Gd3	346.6(1)
					3	Gd2	349.4(1)
					1	O	399.7(1)
				O:	6	Gd1	259.3(1)

Acknowledgements
We thank Dipl.-Chem. *F.M. Schappacher* for the work at the scanning electron microscope. This work was financially supported by the Deutsche Forschungsgemeinschaft.

References

1. Dzevenko MV, Zaremba R, Hlukhyy V, Rodewald UCh, Pöttgen R, Kalychak YaM (2007) Z Anorg Allg Chem 633:724
2. Zaremba R, Pöttgen R (2007) J Solid State Chem 180:2452
3. Zaremba R, Rodewald UCh, Zaremba VI, Pöttgen R (2007) Z Naturforsch 62b:1397
4. Zaremba R, Rodewald UCh, Hoffmann R-D, Pöttgen R (2007) Monatsh Chem 138:523
5. Tuncel S, Hoffmann R-D, Chevalier B, Matar SF, Pöttgen R (2007) Z Anorg Allg Chem 633:151
6. Tuncel S, Chevalier B, Matar SF, Pöttgen R (2007) Z Anorg Allg Chem 633:2019
7. Tuncel S, Rodewald UCh, Chevalier B, Pöttgen R (2007) Z Naturforsch 62b:642
8. Doğan A, Rayaprol S, Pöttgen R (2007) J Phys: Condens Matter 19:076213
9. Donohue J (1974) The Structures of the Elements. Wiley, New York
10. Bobet J-L, Chevalier B, Tuncel S, Pöttgen R (2007) unpublished results
11. Pöttgen R, Gulden Th, Simon A (1999) GIT Labor Fachzeitschrift 43:133
12. Yvon K, Jeitschko W, Parthé E (1977) J Appl Crystallogr 10:73
13. Sheldrick GM (1997) SHELXL-97, Program for Crystal Structure Refinement, University of Göttingen
14. Flack HD, Bernadinelli G (1999) Acta Crystallogr 55A:908
15. Flack HD, Bernadinelli G (2000) J Appl Crystallogr 33:1143
16. Kalychak YaM, Zaremba VI, Pöttgen R, Lukachuk M, Hoffmann R-D (2005) Rare Earth-Transition Metal-Indides. In: Gschneider KA Jr, Pecharsky VK, Bünzli J-C (eds) Handbook on the Physics and Chemistry of Rare Earths, Vol. 34. Elsevier, Amsterdam, chapter 218, p 1
17. Rayaprol S, Heying B, Pöttgen R (2006) Z Naturforsch 61b:495
18. Rodewald UCh, Chevalier B, Pöttgen R (2007) J Solid State Chem 180:1720
19. Dariel MP, Pickus MR (1976) J Less-Common Met 50:125
20. Melamud M, Dariel MP, Shaked H (1979) J Appl Phys 50:1978
21. Snyder GJ, Simon A (1994) Angew Chem 106:713